published in: Journal of the European Ceramic Society 39 (2019) 4874-4881

Thermochemical stability of Fe- and Co-functionalized perovskite-type $SrTiO_3$ oxygen transport membrane materials in syngas conditions

Yang Liu [a], Vladimir Motalov[b,c], Stefan Baumann[a*], Dmitry Sergeev[b], Michael Müller[b], Yoo Jung Sohn[a], Olivier Guillon[a,d]

[a] Forschungszentrum Jülich GmbH, Institute of Energy and Climate Research – Materials Synthesis and Processing (IEK-1), 52425 Jülich, Germany

[b] Forschungszentrum Jülich GmbH, Institute of Energy and Climate Research – Microstructure and Properties of Materials (IEK-2), 52425 Jülich, Germany

[c] Ivanovo State University of Chemistry and Technology, Research Institute of Thermodynamics and Kinetics, 153000 Ivanovo, Russia

[d] Jülich Aachen Research Alliance: JARA-Energy, 52425 Jülich, Germany

Abstract

The materials typically used for oxygen transport membranes, $Ba_{0.5}Sr_{0.5}Co_{0.8}Fe_{0.2}O_{3-\delta}$ (BSCF) and $La_{0.6}Sr_{0.4}Co_{0.2}Fe_{0.8}O_3$ (LSCF) tend to decompose due to their low thermochemical stability under reducing atmosphere. Fe- and Co-doped $SrTiO_3$ ($SrTi_{1-x-y}Co_xFe_yO_{3-\delta}$, $x+y \leq 0.35$) (STCF) materials showing an oxygen transport comparable to LSCF have great potential for application in ion-transport-devices. In this study, the thermochemical stability of pure perovskite-structured STCF was investigated after annealing in a syngas atmosphere at 600–900 °C. The phase composition of the materials after annealing was characterized by means of X-ray diffraction (XRD). The thermodynamic activities of SrO, FeO, and CoO in the STCF materials were evaluated using Knudsen effusion mass spectrometry (KEMS). Co-doped $SrTiO_3$ (STC) materials were not stable after annealing in the syngas atmosphere above 5 mol% Co-substitution. Ruddlesden-Popper-like phases and $SrCO_3$ were detected after annealing at 600 °C. In contrast, Fe substitution (STF) showed good stability after annealing in syngas upto 35 mol% substitution.

Keywords

strontium titanate; thermochemical stability; syngas; oxygen transport membrane; Knudsen Effusion Mass Spectrometry

published in: Journal of the European Ceramic Society 39 (2019) 4874-4881

1 Introduction

Functional ceramics with mixed ionic–electronic conductivity (MIEC) are key materials in various emerging energy technologies such as solid oxide fuel or electrolysis cells (SOFCs/SOECs), or oxygen transport membranes (OTMs) for the generation of pure oxygen or commodity chemicals and synthetic fuels in membrane reactors [1]-[3]. In particular, materials used in membrane reactors must exhibit good stability at high temperatures and in harsh atmospheres, e.g. low oxygen partial pressure and/or corrosive gases such as CO_2, CO, and H_2. Therefore, a good compromise between performance and long-term stability must be found.

Perovskite-type oxides often provide high MIEC. In particular, cobaltites and ferrites such as $SrCo_{0.8}Fe_{0.2}O_{3-\delta}$ (SCF), $La_{1-x}Sr_xCo_{1-y}Fe_yO_{3-\delta}$ (LSCF) and $Ba_{0.5}Sr_{0.5}Co_{0.8}Fe_{0.2}O_{3-\delta}$ (BSCF) have been widely investigated as membranes as well as oxygen reduction electrodes (cathodes) for SOFCs, and have performed well [4]-[9]. However, these materials have a low chemical and structural stability under low oxygen partial pressure and acid gases such as CO_2 [10]-[13], which hinders their use e.g. in membrane reactors. In addition, $Ba_{0.5}Sr_{0.5}Co_{0.8}Fe_{0.2}O_{3-\delta}$ (BSCF) presents slow deterioration at temperatures below 825 °C [12] and starts to decompose at 600 °C and above in a 4% H_2 (in argon) atmosphere [13]. It was found that partially substituting the B site of SCF with a fixed-valence-state cation such as Al [14],[15], Zr [16], Ta [17], Nb [5],[18], Y [19],[20], W [21], and Ti [22]-[26] could effectively reduce oxygen stoichiometry variations, suppress thermal and chemical expansion, and improve stability. However, the modified materials still lack stability under reducing atmospheres such as syngas, i.e. a mixture of H_2 and CO with some CO_2 and H_2O content.

In contrast, $SrTiO_3$ (STO) is a very stable perovskite-type oxide [27],[28] that is of particular interest due to the fact that aliovalent cation doping of the A or B site can induce either electronic or ionic conductivity, or both. For MIEC in particular, iron and/or cobalt are of interest as B-site dopants in STO [29]-[37]. Our previous work shows that the STO materials lightly doped with Co and Fe, i.e. max 35 mol% B-site substitution, obtained a comparable permeation rate to LSCF while maintaining good chemical stability and decreasing the coefficient of thermal expansion [34],[38]. At high temperatures (≥800 °C), Fe or Co doping resulted in comparable permeation rates, whereas at lower temperatures (<800 °C), Co doping showed superior performance due to higher catalytic activity [34],[38].

However, there are still gaps in knowledge regarding high-temperature chemistry and the thermochemical stability of these materials in an operation-relevant atmosphere, i.e. syngas derived from partial oxidation of methane. In this study, therefore, the phase stability of $SrTi_{1-x-}$

$_yCo_xFe_yO_{3-\delta}$ (STCF) materials after annealing in a syngas atmosphere at 600–900 °C was investigated. In addition, in order to study if the decomposition mechanism of STCF materials is related to oxide activity, the thermodynamic activities of the oxide components were evaluated on the basis of the mass spectra of STCF and pure SrO, CoO, and FeO obtained using Knudsen effusion mass spectrometry (KEMS).

2 Experimental

2.1 Powder synthesis

The perovskite-structured STCF powders were synthesized using the Pechini method. The process is described in detail in our previous papers [34],[38]. All of the powders were calcined at 1000 ˚C for 2 h in order to obtain phase purity. The mean particle size d_{50} was around 2 μm and the specific surface area was 1–5 m^2/g for all powders.

2.2 Annealing in syngas

The annealing experiments with the powders were conducted using an in-house set-up with four tubes. A detailed description can be found in [39]. This set-up made it possible to anneal samples at four different temperatures in the same feed gas, equilibrating at the selected temperatures in the different tubes. The calcined STCF powders were loosely pressed into pellets and placed in alumina boats in the four tubes, which were heated at 5 K/min to 600 °C, 700 °C, 800 °C, and 900 °C, respectively, in air. After each tube reached the target temperature, N_2 was flushed through to remove oxygen from the tubes. The mixed and well-distributed feed gas, consisting of 33.3% CO, 53.3% H_2, and 13.4% H_2O, was then sent to the tubes with a total flow rate of 100 ml/min. The calculated gas composition in equilibrium at the different temperatures is shown in Table 1, based on the assumption that the syngas achieved equilibrium at each temperature due to relatively low space velocities and consequently long residence times. After 72 h annealing in the syngas, nitrogen was flushed through the tubes again and the samples were cooled to room temperature (RT) with continuous N_2 flushing.

Table 1 Calculated gas composition of the annealing syngas at various temperatures

Gas	600 °C	700 °C	800 °C	900 °C
H_2	45.1%	54.5%	57.5%	57.2%
CO	10.9%	24.8%	28.4%	29.4%

H_2O	21.0%	10.0%	8.9%	9.5%
CO_2	13.7%	7.4%	4.8%	3.9%
CH_4	9.3%	3.2%	0.4%	0
O_2 (bar)	$3*10^{-25}$	$5*10^{-23}$	$1*10^{-20}$	$1*10^{-18}$
Graphite	Yes	0	0	0

The experimental investigations were complemented by thermodynamic calculations performed using the software package FactSage 7.1 (GTT Technologies, Herzogenrath, Germany). The databases used were the commercial Fact and SGTE databases included in the software package.

2.3 Knudsen effusion mass spectrometer experiments

KEMS is an established vapour pressure measurement technique that combines the Knudsen effusion method with mass spectrometric analysis of evaporation products [40]. The experiments were carried out in a single-focusing CH5 magnetic mass spectrometer (Varian MAT, Bremen). Details of the instrument are given in the literature [41]. The samples were loaded into an iridium Knudsen cell with inner dimensions of 7 mm (diameter) x 8 mm (height), which had a channel-type effusion orifice with a diameter of 0.3 mm and a length of 0.5 mm. The cell was placed inside a massive tungsten envelope to ensure uniform temperature distribution. The cell was heated by radiation or electron bombardment from the tungsten resistance furnace. The temperature of the cell was monitored in a black-body hole at the bottom of the tungsten envelope using an automatic optical pyrometer (Dr. Georg Maurer GmbH, Kohlberg) calibrated by the melting points of the pure metals Ag, Cu, Ni, and Pt. The accuracy of the temperature measurement was ±3 K. The gaseous species effusing from the cell, which were in equilibrium with the condensed phase of the sample, were ionized by electrons with an energy of 70 eV and an emission current of 0.1 mA. A movable molecular beam shutter placed between the cell and the ionization chamber made it possible to distinguish species effusing from the cell from those of the background. The ions formed in the ionization chamber were focused using an ion-optical system and accelerated with a negative potential of 8000 V to a 90 º magnetic sector field, where they were separated according to their mass-to-charge ratio (m/z). Ion current intensity was measured by a secondary MC12/17 electron multiplier (MasCom) operating in DC mode. A metallic valve separating the ion source and the Knudsen cell

chambers provided a rapid exchange of the sample in the cell whilst keeping the ion source running under high vacuum. By this means, the day-to-day fluctuations of the sensitivity constant of the mass spectrometer were typically below 5%.

The STC, STF, and STCF samples as well as the pure oxides SrO (99.5%, Alfa Aesar), CoO (99.995%, Alfa Aesar), and FeO (99.9%, Aldrich) were studied in the overall temperature range of 1720–1880 °C.

2.4 Phase composition characterization

The phase compositions of as-synthesized and annealed powders were characterized by means of X-ray diffraction (XRD) using a D4 ENDEAVOR diffractometer with Cu K_α radiation (Bruker) with a step size of 0.02° and 0.75 s/step from 10 to 80° (2θ). The data was then analysed with the X'Pert Highscore program package (PANalytical B.V., version 3.0.5). Phase quantification of the materials was determined using the Rietveld refinement method with TOPAS computer software. In addition, the XRD patterns of the STCF powders after the KEMS experiment were recorded for qualitative phase analysis.

3 Results and discussion

3.1 Annealing of STCF in syngas

The synthesized STCF powders exhibited a pure perovskite structure, as shown in Figure 1, which depicts the XRD patterns of $SrTi_{0.75}Fe_{0.25}O_{3-\delta}$ (STF25), $SrTi_{0.75}Fe_{0.125}Co_{0.125}O_{3-\delta}$ (STC12.5F12.5), $SrTi_{0.75}Co_{0.25}O_{3-\delta}$ (STC25), and $SrTi_{0.95}Co_{0.05}O_{3-\delta}$ (STC05).

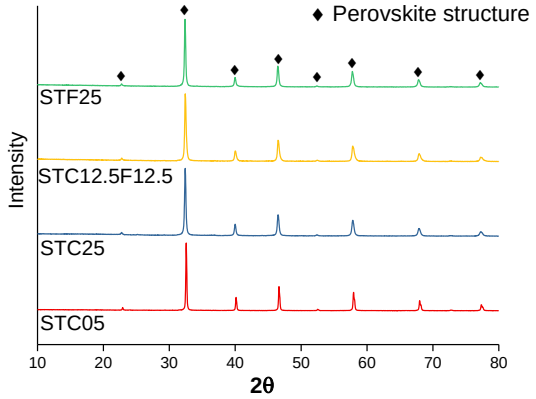

Figure 1 XRD patterns of synthesized $SrTi_{0.75}Fe_{0.25}O_{3-\delta}$ (STF25), $SrTi_{0.75}Fe_{0.125}Co_{0.125}O_{3-\delta}$ (STC12.5F12.5), $SrTi_{0.75}Co_{0.25}O_{3-\delta}$ (STC25), and $SrTi_{0.95}Co_{0.05}O_{3-\delta}$ (STC05) powder.

The phase composition of the STCF samples after annealing at 600 °C and 900 °C was analysed. Figure 2 shows the XRD patterns of STCF powders after annealing at 600 °C and 900 °C, respectively. Table 2 shows the quantitative XRD analysis of annealed samples at 600 °C. If Co substitution stayed below 5 mol%, a pure perovskite phase was maintained. Above 5 mol% Co substitution, additional peaks of Co_3O_4 and $SrCO_3$ could be detected. The decomposition of perovskite STC25 can be explained by the very low p_{O2} (~10^{-25} bar), which reduced some of the Co cations to the metallic state [42]. These atoms were therefore extracted from the oxide lattice. However, in the cooling phase of the experiment the tube was flushed with nitrogen leading to an increased p_{O2} (~10^{-5} bar) sufficient to instantaneously re-oxidise the cobalt to Co_3O_4 [43] as found in the post-test XRD analysis. The excess SrO from the A site then formed $SrCO_3$ in the CO_2-containing atmosphere. In contrast, the STF25 materials showed phase stability, with no secondary phases detected after syngas annealing at 600 °C. The STC12.5F12.5 material presented a perovskite structure percentage value between STC25 and STF25, showing that Fe functionalization of STO reveals higher phase stability compared to Co functionalization in the syngas atmosphere at 600 °C.

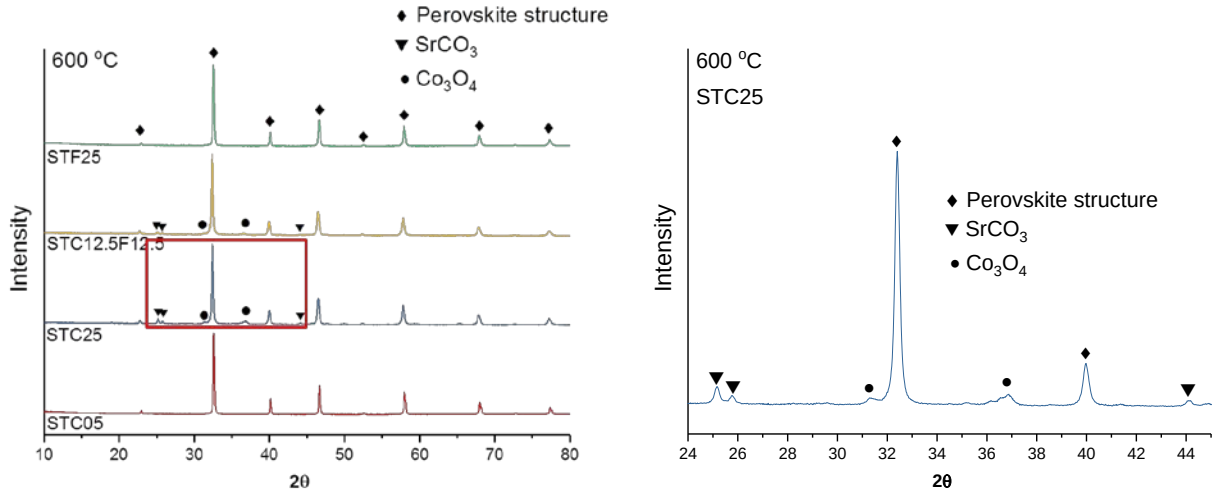

a) b)

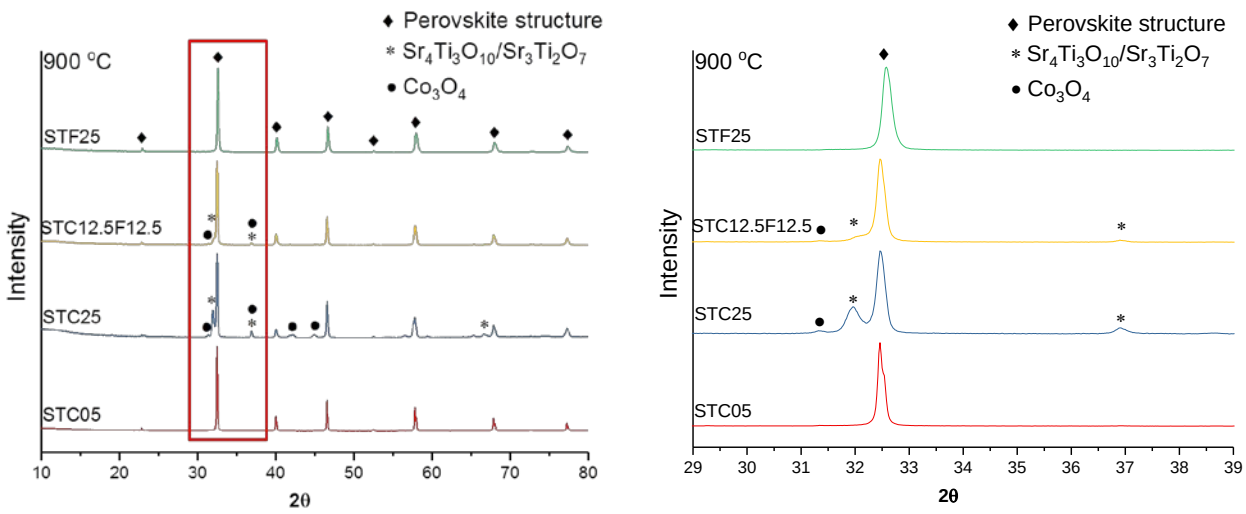

c) d)

Figure 2 XRD patterns of STC05, STC25, STC12.5F12.5, and STF25 after annealing in the syngas at (a) 600 °C and (c) 900 °C. (b) and (d) are partial zooms of (a) and (c), respectively. The red rectangles in a) and c) represent the corresponding zoom areas in b) and d).

Table 2 Phase composition (wt.%) of the samples after annealing, obtained from Rietveld refinement of XRD data

600 °C	STC05	STC25	STC35	STF25	STC12.5F12.5	STF35
Perovskite	100%	80%	67%	100%	92%	91%
Co_3O_4	0	9%	12%	0	3%	3% Fe_3O_4
$SrCO_3$	0	11%	21%	0	5%	6%
900 °C	STC05	STC25	STC35	STF25	STC12.5F12.5	STF35
Perovskite	100%	44%	17%	100%	83%	100%
Co_3O_4	0	9%	12%	0	4%	0
$Sr_4Ti_3O_{10}$	0	26%	33%	0	13%	0
$Sr_3Ti_2O_7$	0	21%	38%	0	0	0

At 900 °C, the p_{O2} (10^{-18} bar) is higher than at 600 °C but still very low. Again, STC05 was fully stable, but Co was easily extracted from STC with higher Co content. In contrast to 600 °C, Ruddlesden-Popper-like phases, i.e. $Sr_4Ti_3O_{10}$ and $Sr_3Ti_2O_7$, formed instead of $SrCO_3$ in order to

compensate for the loss of B-site cations. $SrCO_3$ is less stable at 900 °C compared to 600 °C under low partial pressure [44],[45] and apparently the Ruddlesden-Popper-like phases show superior stability in such conditions.

FactSage calculations were performed to confirm the experimental results and the proposed decomposition mechanism and subsequent temperature dependant formation of $SrCO_3$ or Ruddlesden-Popper-like phases. Since the available commercial databases do not contain doped $SrTiO_3$ phases, the stability of pure $SrTiO_3$ in the used syngas at 600-1000 °C was calculated. The calculations reveal that $SrTiO_2$ is the only stable phase under these conditions. To consider the excess of SrO in STC after annealing caused by the reduction and subsequent extraction of Co from the B-site sub-lattice, the stability of "$SrO*(TiO_2)_{0.9}$" was calculated under the same conditions. Below 658 °C $SrCO_3$ is stable beside $SrTiO_3$. Above 658 °C $Sr_4Ti_3O_{10}$ is stable beside $SrTiO_3$, causing also a respective reduction of the amount of $SrTiO_3$ in comparison to lower temperatures. These results are in very good agreement with the experimental findings.

Figure 3 shows the amount of the remaining perovskite structure weight percentage of STC and STCF after annealing, in dependence on Co content at 600 ˚C and 900 ˚C. At both temperatures, the perovskite structures decomposed more severely with increasing Co content, because Co is easier to reduce than Fe [46]. After 72 h annealing, the remaining perovskite percentage at 600 ˚C was much higher than that at 900 ˚C. It should be noted that this does not reveal a higher stability of the perovskite phase at 600 °C, but rather that the decomposition kinetics are much slower.

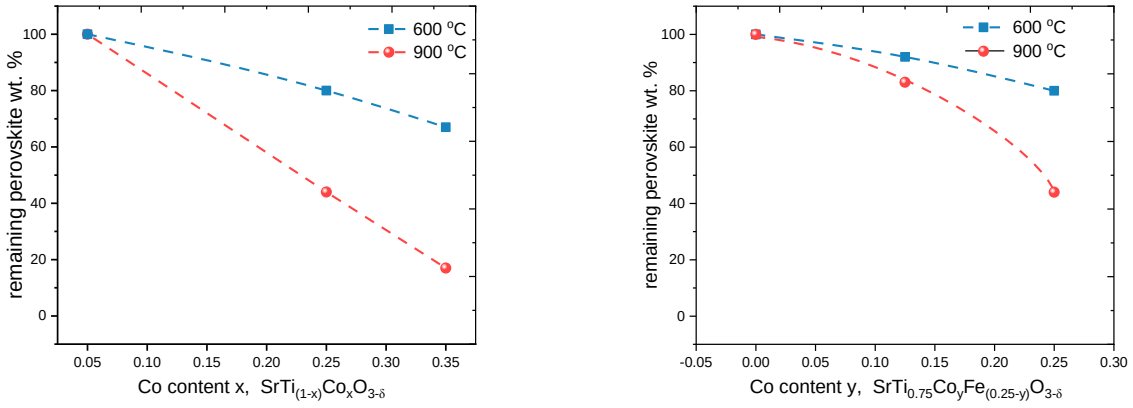

a) b)

Figure 3 Percentage of the perovskite structure of the (a) STC and (b) STCF samples after annealing at 600 °C and 900 °C, respectively. The dashed lines here are for guidance only and do not represent a model.

3.2 Vaporization of STCF in a KEMS experiment

Based on the results of the annealing experiments and thermodynamic calculations it is proposed that the decomposition of STC is caused by the reduction and subsequent extraction of Co. However, the dopants could also influence the activity of the contained oxides in the perovskite phase and thus change the stability. Since there are no activity data on doped $SrTiO_3$ available from literature to the knowledge of the authors, the activities were determined by KEMS experiments to elucidate a respective contribution of activity changes by dopants to the stability in syngas.

The measurements were conducted at temperatures above 1700 °C due to the relatively low vapour pressures of the perovskites at lower temperatures. Although these temperatures are much higher than the temperatures in the annealing experiments, the results are relevant for the interpretation of the annealing experiments since the perovskite structure is stable in the entire temperature range.

3.2.1 Mass spectra

The primary ions O^+, O_2^+, M^+, and MO^+ as well as the doubly charged ions M^{++} were detected in the mass spectra of the vapour over pure oxides and the different STC, STF, and STCF samples (M = Sr, Co for STC; M = Sr, Fe for STF; and M = Sr, Co, and Fe for STCF). In addition, the minor ion peaks Ir^+, WO^+, WO_2^+, $SrWO_3^+$, and $SrWO_4^+$ were registered, which do not relate to the samples studied but rather to the cell material and the products of interaction of the tungsten envelope with the Sr-O vapours outside the Knudsen cell. Among the primary ions, MO^+ ions are the most important since they are formed by ionization from the MO molecules and can be directly used for MO activity calculation. The non-fragment origin of the SrO^+ ion was confirmed by its low appearance energy of 6.4 ± 0.5 eV (SrO ionization energy is 6.6 eV [47]) found by linear extrapolation of the dependence of ion current vs energy of ionizing electrons in the ionization efficiency curve (IEC), shown in Figure 4. The SrO^+ IECs were identical as measured in three objects with the substantially varying ion current ratios $SrO^+/SrWO_4^+$, i.e. 2, 7, and 16 for STF35, STF25, and pure SrO, respectively. Thus, fragment

contribution to the SrO^+ ion current from the outside ternary $SrWO_4$ molecules can be neglected. Analogously, the other MO^+ ions (M = Co, Fe) were also assumed to be molecular.

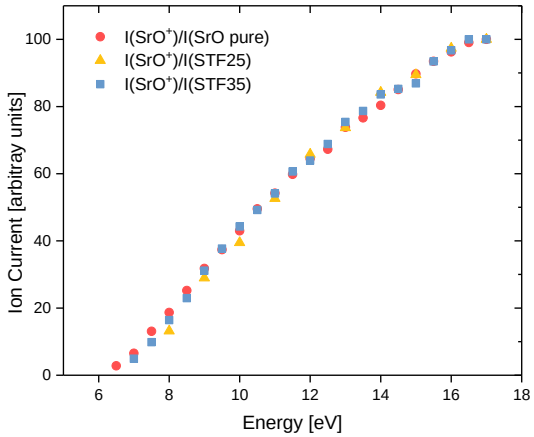

Figure 4 Ionization efficiency curves for SrO^+

In Figure 5, the temperature dependencies of ion currents in the form $\ln(IT) = f(1000/T)$ are shown as example for pure SrO and STC35. In these coordinates, the dependencies should be straight Clausius-Clapeyron lines. The measurements were carried out during heating (3 points) and cooling (2 points). It can be seen that all ion currents in SrO are reproducible during heating and cooling cycles, indicating congruent vaporization. In contrast, most ion currents in STC35 are not reproducible. $I(O^+)$, $I(O_2^+)$, $I(Co^+)$, and $I(CoO^+)$ decrease considerably during cooling whereas $I(Sr^+)$ increases and $I(SrO^+)$ remains practically the same. Such time evolution of ion currents indicates the incongruent vaporization of the STC35 sample and its gradual decomposition. Very similar non-reproducible heating and cooling temperature dependencies were obtained for all other STC, STF, and STCF samples; only $I(SrO^+)$ was more or less reproducible indicating the practical constancy of the activity of SrO in these samples in the course of their decomposition.

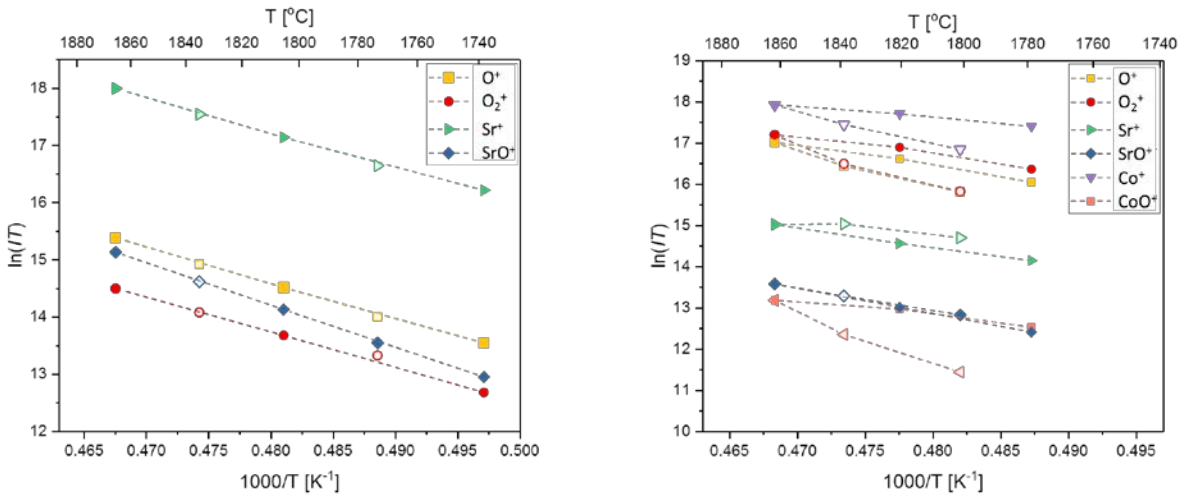

a) b)

Figure 5 Temperature dependence of ion currents in (a) SrO and (b) STC35; points measured during heating and cooling are shown by solid and open symbols, respectively

3.2.2 Thermodynamic activity

Thermodynamic activity (*a*) of the individual oxides MO (M = Sr, Co, and Fe) in STC, STF, and STCF samples was determined by ion current comparison, evaluated using the consideration of heterophase equilibrium

$$\mathrm{MO(cr)} = \mathrm{MO\ (g)} \tag{1}$$

whose equilibrium constant is written as

$$K_p(2) = p^{\mathrm{o}}(\mathrm{MO}) = \frac{p^{\mathrm{s}}(\mathrm{MO})}{a(\mathrm{MO})} \tag{2}$$

where *p* is the vapour pressure, and the indexes “s” and “o” relate to the studied sample and pure oxide, respectively. Using the relation between pressure and ion current intensity

$$p_i = k_i I_i T \tag{3}$$

where *I* is the intensity of ion current, k_i is the sensitivity constant of the mass spectrometer for the species *i,* we get the thermodynamic activity $a(\mathrm{MO})$

$$a(\mathrm{MO}) = \frac{p^{\mathrm{s}}(\mathrm{MO})}{p^{\mathrm{o}}(\mathrm{MO})} = \frac{I^{\mathrm{s}}(\mathrm{MO})}{I^{\mathrm{o}}(\mathrm{MO})} \tag{4}$$

Vaporization of pure SrO was repeated from time to time during the experimental cycle with the STC, STF, and STCF samples. Altogether five runs of pure SrO were obtained, which show a reproducibility of ion currents within ±10% on an average. Therefore, the doubled value (±20%) can be accepted as the overall uncertainty of the activity measurements. The SrO activities of STCF samples obtained in different runs, each with a fresh portion of the sample, agree within the estimated uncertainty. Figure 6 shows an example for $a(\mathrm{SrO})$ of STF35. The comparison of activities within the separate groups (STF, STC, or STCF), as shown in Figure 7 (a-c), does not generally reveal any differences depending on composition; the only slight difference detected was for STF25 and STF35. At the same time, the differences between the values in the STF, STC, and STCF groups (see Figure 7 (d)) are more apparent, although they are also not large. Table 3 lists the average SrO activity values of these three groups at 1827 °C. Considering the uncertainty, the values are very close to each other as well as to the values measured for the undoped $SrTiO_3$ phases shown in the same table. These facts indicate that

(1) the SrO activity in $SrTiO_3$ is not very sensitive to doping by Co or Fe and

(2) SrO activity does not depend on the dopant concentration within the studied composition range.

Therefore, the instabilities of the STC, STF, and STFC samples observed in the annealing experiments (Section 3.1) depending on the dopant amount can hardly be associated with the SrO activity. This conclusion is also supported by the fact that the tendency of the SrO activity to increase in the STF-STC-STCF series does not correlate with the relative stabilities of the samples in the annealing experiments with a fixed amount of dopant (in particular, 25%, see Table 2).

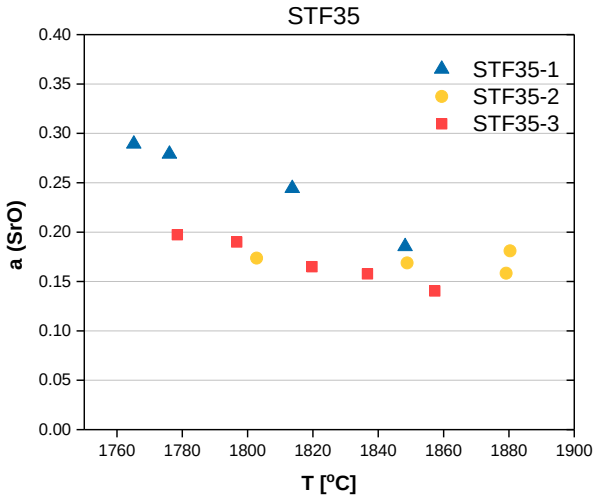

Figure 6 Activity of SrO measured in different runs with the STF35 sample

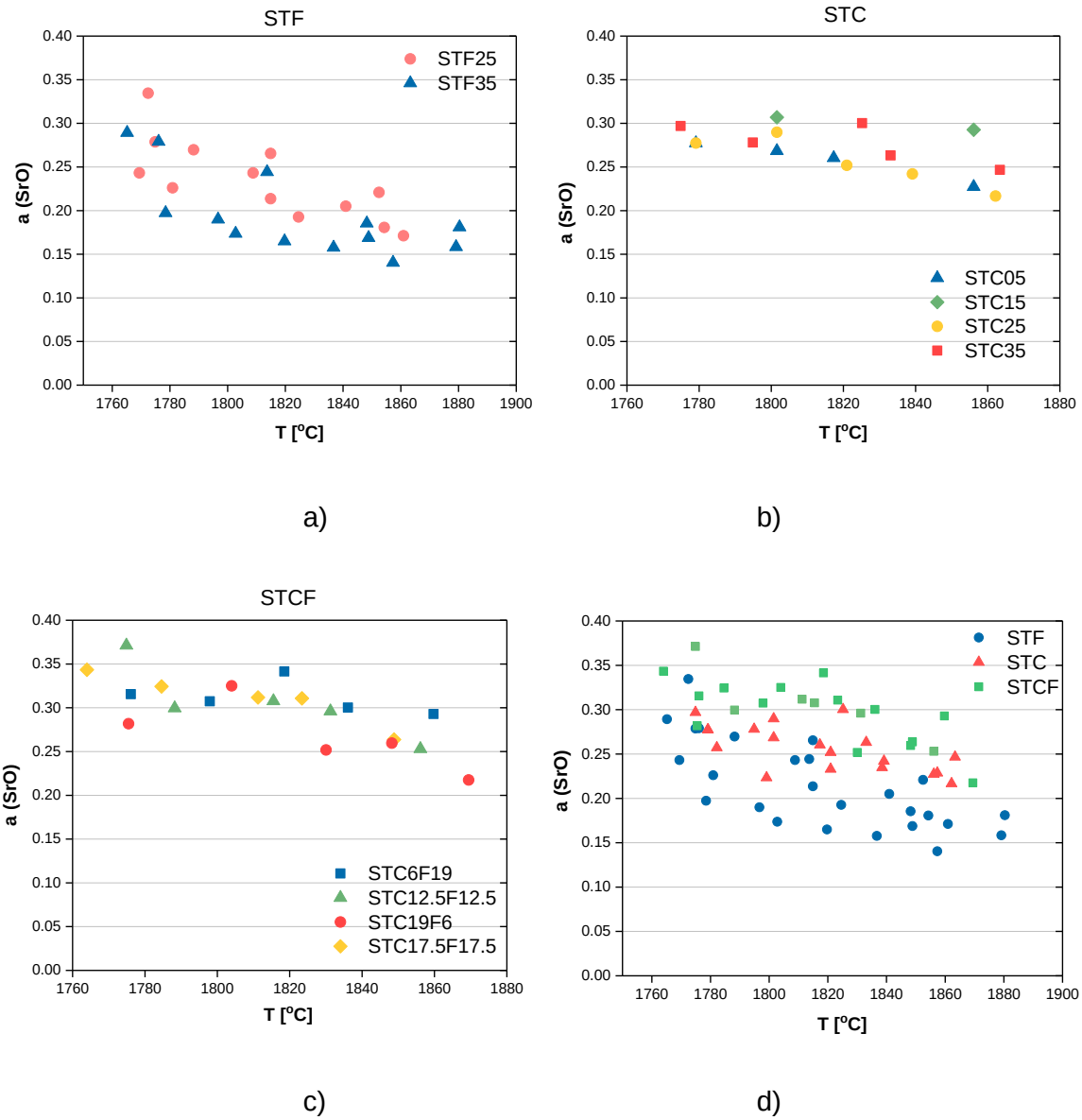

Figure 7 Activity of SrO measured in (a) STF, (b) STC, and (c) STCF samples of different composition. (d) Activity of SrO measured in the STF, STC, and STCF groups.

Table 3 $a(\mathrm{SrO})$ values in STC, STF and STCF at 1827 °C

STF	STC	STCF	$Sr_{0.9}TiO_3$	$Sr_{1.1}TiO_3$
0.21±0.04	0.26±0.05	0.29±0.06	0.21±0.04	0.27±0.05

In Figure 8, the activities of FeO and CoO in STF, STC, and STCF are shown. It can be seen that they both decrease during heating and cooling cycles (actually in time, see discussion of Figure 5b), thereby reflecting the gradual change in composition of the samples in the course of the vaporization experiments. The decrease is much more pronounced (by order of magnitude) for CoO than for FeO. These facts indicate that Co is mainly responsible for the samples' instability in the KEMS experiments. This also correlates with the higher instability of STC and STCF samples compared to STF in the annealing experiments (Section 3.1).

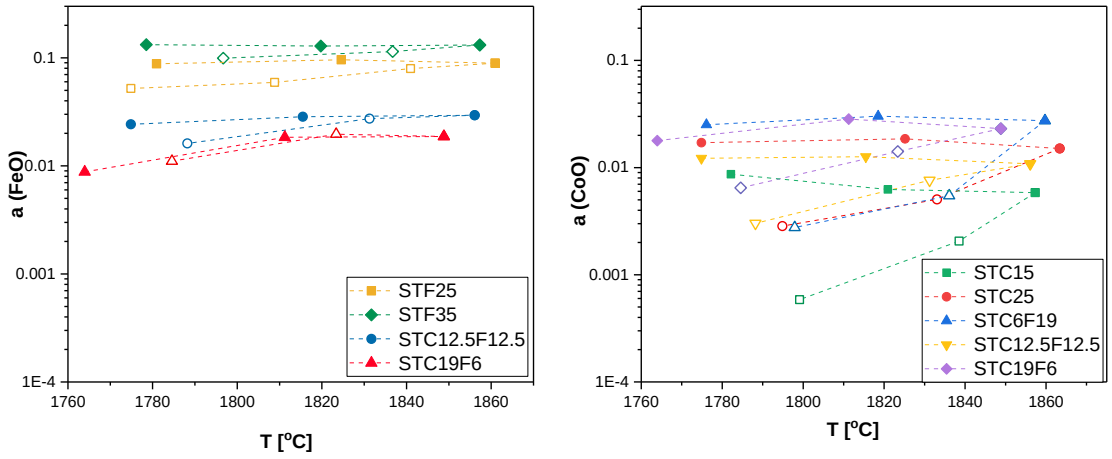

a) b)

Figure 8 Activity of (a) FeO and (b) CoO in STF, STC, and STCF; points measured during heating and cooling are shown by solid and open symbols, respectively.

3.2.3 Phase composition of the samples after KEMS measurement

STCF samples were characterized by XRD after the KEMS measurements at 1720–1880 °C. In addition to the perovskite structure, Ruddlesden-Popper-like phases i.e. $Sr_4Ti_3O_{10}$, $Sr_3Ti_2O_7$ and Sr_2TiO_4 were detected, as shown in Figure 9. This result further confirmed the partial decomposition of STCF materials during the evaporation, as discussed in Section 3.2.2. In contrast to the annealing experiments (Section 3.1), not only the STC materials decomposed but also STF25 decomposed due to the very high temperatures and sufficiently low p_{O2}, which reduced some of the Fe cations to the metallic state. According to equilibrium calculations the p_{O2} above strontium titanates in the Knudsen cell at 1880 °C is about $3*10^{-8}$ bar, while iron oxide is already reduced to metallic iron below $4.5*10^{-7}$ bar. Furthermore, incongruent vaporisation at high temperatures, as discussed in Section 3.2.1, leads to depletion of iron.

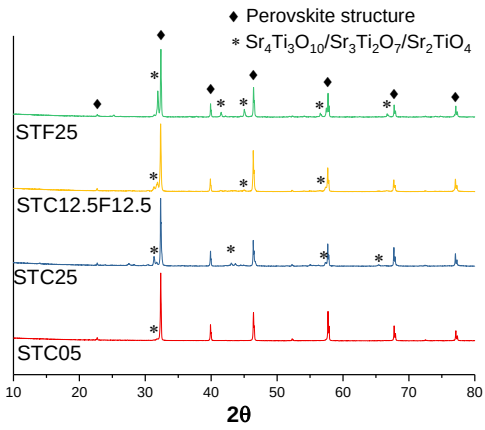

Figure 9 XRD pattern of the STCF samples after the KEMS measurement

4 Conclusions

In this study, the thermochemical stability of $SrTi_{1-x-y}Co_xFe_yO_{3-\delta}$ (STCF, $x+y\leq0.35$) materials after annealing in syngas atmosphere at 600 °C and 900 °C was characterized by XRD. Ruddlesden-Popper-like phases and Co_3O_4 were detected in STC materials after annealing at 900 °C. In addition to the Ruddlesden-Popper-like phases, the $SrCO_3$ phase was detected in the STC materials after annealing at 600 °C. In contrast, STF materials maintained a perovskite structure after annealing. In particular, at 900 °C, only the STF perovskite structure was detected. Thermodynamic activities of the oxide components such as SrO, CoO, and FeO of STCF were evaluated from the mass spectra to further analyse the reason for decomposition. KEMS results showed that the SrO activity in $SrTiO_3$ is not very sensitive to doping by Co or Fe within the studied composition range. This suggests that the instabilities of the STC, STF, and STFC samples observed in the annealing experiments depending on the dopant amount cannot be associated with the SrO activity. We conclude that the decomposition of STC occurs in two steps. First, Co is reduced to the metallic state and, hence, extracted from the perovskite structure in a reducing atmosphere ($P_{O2}=10^{-18}$-10^{-25} bar), leading to the decomposition of perovskite structure and the formation of the Ruddlesden-Popper structure. Then, CO_2 reacts with the SrO in the Ruddlesden-Popper structure, resulting in the $SrCO_3$ phase at 600 °C.

STF materials maintained their perovskite structure after annealing in reducing and CO_2-containing atmosphere, highlighting good phase stability and exhibiting excellent potential for application as separation materials in membrane reactors and solid oxide fuel cells.

5 Acknowledgement

We would like to thank the China Scholarship Council (CSC) for providing financial support for this work. The authors thank Mr. S. Heinz and Dr. Falk Schulze-Küppers for technical assistance in sample preparation (all Forschungszentrum Juelich GmbH, IEK-1). V. Motalov thanks the Ministry of Education and Science of the Russian Federation for support in the framework of project no. 4.3232.2017/4.6.

References

[1] X. Meng, X. Bi, B. Meng, N. Yang, X. Tan, L. Liu, S. Liu, $H_2/CH_4/CO_2$-tolerant properties of $SrCo_{0.8}Fe_{0.1}Ga_{0.1}O_{3-\delta}$ hollow fiber membrane reactors for methane partial oxidation to syngas, Fuel Processing Technology 161 (2017) 265-272.

[2] Y. Liu, X. Zhu, W. Yang, Stability of sulfate doped $SrCoO_{3-\delta}$ MIEC membrane, Journal of Membrane Science 501 (2016) 53-59.

[3] Y. Zheng, J. Wang, B. Yu, W. Zhang, J. Chen, J. Qiao, J. Zhang, A review of high temperature co-electrolysis of H_2O and CO_2 to produce sustainable fuels using solid oxide electrolysis cells (SOECs): advanced materials and technology, Chemical Society Reviews 46(5) (2017) 1427-1463.

[4] F. Schulze-Küppers, S. Baumann, F. Tietz, H.J.M. Bouwmeester, W.A. Meulenberg, Towards the fabrication of $La_{0.98-x}Sr_xCo_{0.2}Fe_{0.8}O_{3-\delta}$ perovskite-type oxygen transport membranes, Journal of the European Ceramic Society 34(15) (2014) 3741-3748.

[5] S. Wang, F. Jin, L. Li, R. Li, B. Qu, T. He, Stability, compatibility and performance improvement of $SrCo_{0.8}Fe_{0.1}Nb_{0.1}O_{3-\delta}$ perovskite as a cathode for intermediate-temperature solid oxide fuel cells, International Journal of Hydrogen Energy 42(7) (2017) 4465-4477.

[6] Z. Chen, R. Ran, W. Zhou, Z. Shao, S. Liu, Assessment of $Ba_{0.5}Sr_{0.5}Co_{1-y}Fe_yO_{3-\delta}$ (y=0.0-1.0) for prospective application as cathode for IT-SOFCs or oxygen permeating membrane, Electrochimica Acta 52(25) (2007) 7343-7351.

[7] S. McIntosh, J.F. Vente, W.G. Haije, D.H.A. Blank, H.J.M. Bouwmeester, Structure and oxygen stoichiometry of $SrCo_{0.8}Fe_{0.2}O_{3-\delta}$ and $Ba_{0.5}Sr_{0.5}Co_{0.8}Fe_{0.2}O_{3-\delta}$, Solid State Ionics 177(19) (2006) 1737-1742.

[8] Z. Shao, G. Xiong, J. Tong, H. Dong, W. Yang, Ba effect in doped $Sr(Co_{0.8}Fe_{0.2})O_{3-\delta}$ on the phase structure and oxygen permeation properties of the dense ceramic membranes, Separation and Purification Technology 25(1) (2001) 419-429.

[9] S. Baumann, J.M. Serra, M.P. Lobera, S. Escolástico, F. Schulze-Küppers, W.A. Meulenberg, Ultrahigh oxygen permeation flux through supported $Ba_{0.5}Sr_{0.5}Co_{0.8}Fe_{0.2}O_{3-\delta}$ membranes. Journal of Membrane Science 377 (2011) 198– 205

[10] Q. Zeng, Y.-b. Zuo, C.-g. Fan, C.-s. Chen, CO_2-tolerant oxygen separation membranes targeting CO_2 capture application, Journal of Membrane Science 335(1) (2009) 140-144.

[11] S. Faraji, K.J. Nordheden, S.M. Stagg-Williams, A comparative study of $Ba_{0.5}Sr_{0.5}Co_{0.8}Fe_{0.2}O_x$ (BSCF) and $SrFeCo_{0.5}O_x$ (SFC) ceramic membranes used for syngas production, Applied Catalysis B: Environmental 99(1) (2010) 118-126.

[12] Z. Shao, W. Yang, Y. Cong, H. Dong, J. Tong, G. Xiong, Investigation of the permeation behavior and stability of a $Ba_{0.5}Sr_{0.5}Co_{0.8}Fe_{0.2}O_{3-\delta}$ oxygen membrane, Journal of Membrane Science 172(1) (2000) 177-188.

[13] J. Ovenstone, J.-I. Jung, J.S. White, D.D. Edwards, S.T. Misture, Phase stability of BSCF in low oxygen partial pressures, Journal of Solid State Chemistry 181(3) (2008) 576-586.

[14] Z. Wu, W. Jin, N. Xu, Oxygen permeability and stability of Al_2O_3-doped $SrCo_{0.8}Fe_{0.2}O_{3-\delta}$ mixed conducting oxides, Journal of Membrane Science 279(1) (2006) 320-327.

[15] A.L. Shaula, V.V. Kharton, N.P. Vyshatko, E.V. Tsipis, M.V. Patrakeev, F.M.B. Marques, J.R. Frade, Oxygen ionic transport in $SrFe_{1-y}Al_yO_{3-\delta}$ and $Sr_{1-x}Ca_xFe_{0.5}Al_{0.5}O_{3-\delta}$ ceramics, Journal of the European Ceramic Society 25(4) (2005) 489-499.

[16] L. Yang, L. Tan, X. Gu, H. Qi, W. Jin, L. Zhang, N. Xu, Effect of the size and amount of ZrO_2 addition on properties of $SrCo_{0.4}Fe_{0.6}O_{3-\delta}$, Aiche J. 49(9) (2003) 2374-2382.

[17] W. Chen, C.-s. Chen, L. Winnubst, Ta-doped $SrCo_{0.8}Fe_{0.2}O_{3-\delta}$ membranes: Phase stability and oxygen permeation in CO_2 atmosphere, Solid State Ionics 196(1) (2011) 30-33.

[18] S.M. Fang, C.Y. Yoo, H.J.M. Bouwmeester, Performance and stability of niobium-substituted $Ba_{0.5}Sr_{0.5}Co_{0.8}Fe_{0.2}O_{3-\delta}$ membranes, Solid State Ionics 195(1) (2011) 1-6.

[19] H. Zhao, N. Xu, Y. Cheng, W. Wei, N. Chen, W. Ding, X. Lu, F. Li, Investigation of Mixed Conductor $BaCo_{0.7}Fe_{0.3-x}Y_xO_{3-\delta}$ with High Oxygen Permeability, The Journal of Physical Chemistry C 114(41) (2010) 17975-17981.

[20] L.-S. Unger, R. Ruhl, M. Meffert, C. Niedrig, W. Menesklou, S.F. Wagner, D. Gerthsen, H.J.M. Bouwmeester, E. Ivers-Tiffée, Yttrium doping of $Ba_{0.5}Sr_{0.5}Co_{0.8}Fe_{0.2}O_{3-\delta}$ part II: Influence on oxygen transport and phase stability, Journal of the European Ceramic Society 38(5) (2018) 2388-2395.

[21] J.Y. Chan, K. Zhang, C. Zhang, H. Tian, S. Liu, Novel tungsten stabilizing $SrCo_{1-x}W_xO_{3-\delta}$ membranes for oxygen production, Ceramics International 41(10, Part B) (2015) 14935-14940.

[22] M. Reichmann, P.M. Geffroy, J. Fouletier, N. Richet, P. Del Gallo, T. Chartier, Effect of cation substitution at the B site on the oxygen semi-permeation flux in $La_{0.5}Ba_{0.5}Fe_{0.7}B_{0.3}O_{3-\delta}$ dense perovskite membranes with B = Al, Co, Cu, Mg, Mn, Ni, Sn, Ti and Zn (part II), Journal of Power Sources 277 (2015) 17-25.

[23] V.V. Kharton, L. Shuangbao, A.V. Kovalevsky, A.P. Viskup, E.N. Naumovich, A.A. Tonoyan, Oxygen permeability and thermal expansion of $SrCo(Ti)O_{3-\delta}$ perovskites, Materials Chemistry and Physics 53(1) (1998) 6-12.

[24] N. Xu, H. Zhao, Y. Shen, T. Chen, W. Ding, X. Lu, F. Li, Structure, electrical conductivity and oxygen permeability of $Ba_{0.6}Sr_{0.4}Co_{1-x}Ti_xO_{3-\delta}$ ceramic membranes, Separation and Purification Technology 89 (2012) 16-21.

[25] J. Tong, W. Yang, R. Cai, B. Zhu, G. Xiong, L. Lin, Investigation on the structure stability and oxygen permeability of titanium-doped perovskite-type oxides of $BaTi_{0.2}Co_xFe_{0.8-x}O_{3-\delta}$ (x=0.2-0.6), Separation and Purification Technology 32(1) (2003) 289-299.

[26] G. Yang, C. Su, Y. Chen, F. Dong, M.O. Tade, Z. Shao, Cobalt-free $SrFe_{0.9}Ti_{0.1}O_{3-\delta}$ as a high-performance electrode material for oxygen reduction reaction on doped ceria electrolyte with favorable CO_2 tolerance, Journal of the European Ceramic Society 35(9) (2015) 2531-2539.

[27] Q. Kang, T. Wang, P. Li, L. Liu, K. Chang, M. Li, J. Ye, Photocatalytic Reduction of Carbon Dioxide by Hydrous Hydrazine over Au-Cu Alloy Nanoparticles Supported on $SrTiO_3/TiO_2$ Coaxial Nanotube Arrays, Angewandte Chemie International Edition 54(3) (2015) 841-845.

[28] Y. Bi, M.F. Ehsan, Y. Huang, J. Jin, T. He, Synthesis of Cr-doped $SrTiO_3$ photocatalyst and its application in visible-light-driven transformation of CO_2 into CH_4, Journal of CO_2 Utilization 12 (2015) 43-48.

[29] X. Li, H. Zhao, N. Xu, X. Zhou, C. Zhang, N. Chen, Electrical conduction behavior of La, Co co-doped $SrTiO_3$ perovskite as anode material for solid oxide fuel cells, International Journal of Hydrogen Energy 34(15) (2009) 6407-6414.

[30] S. Hui, A. Petric, Evaluation of yttrium-doped $SrTiO_3$ as an anode for solid oxide fuel cells, Journal of the European Ceramic Society 22(9) (2002) 1673-1681.

[31] J.R. Jurado, F.M. Figueiredo, B. Gharbage, J.R. Frade, Electrochemical permeability of $Sr_{0.7}(Ti,Fe)O_{3-\delta}$ materials, Solid State Ionics 118(1) (1999) 89-97.

[32] V. Metlenko, W.C. Jung, S.R. Bishop, H.L. Tuller, R.A. De Souza, Oxygen diffusion and surface exchange in the mixed conducting oxides SrTi1-yFeyO3-δ. Phys.Chem.Chem.Phys. 18 (2016) 29495-29505

[33] D.P. Fagg, V.V. Kharton, A.V. Kovalevsky, A.P. Viskup, E.N. Naumovich, J.R. Frade, The stability and mixed conductivity in La and Fe doped $SrTiO_3$ in the search for potential SOFC anode materials, Journal of the European Ceramic Society 21(10) (2001) 1831-1835.

[34] F. Schulze-Küppers, S. Ten Donkelaar, S. Baumann, P. Prigorodov, Y. Sohn, H. Bouwmeester, W. Meulenberg, O. Guillon, Structural and functional properties of $SrTi_{1-x}Fe_xO_{3-\delta}$ ($0 \leqslant x \leqslant 1$) for the use as oxygen transport membrane, Separation and purification technology 147 (2015) 414-421.

[35] A. Murashkina, V. Maragou, D. Medvedev, V. Sergeeva, A.K. Demin, P. Tsiakaras, Electrochemical properties of ceramic membranes based on SrTi0.5Fe0.5O3−δ in reduced atmosphere, International Journal of Hydrogen Energy 37 (2012) 14569-14575.

[36] Y. Kwon, B.T. Na, J.H. Park, K.S. Yun, S.K. Hong, J.H. Yu, J.H. Joo, Guidelines for selecting coating materials for a high oxygen permeation flux in a fluorite-rich dual-phase membrane. Journal of Membrane Science 535 (2017) 200–207

[37] A.A. Murashkina, E.Y. Pikalova, D.A. Medvedev, Gd-doped SrTi0.5Fe0.5O3–δ mixed ionic-electronic conductors: structural, thermal, and electrical properties. Ionics 23 (2017) 2351-2357.

[38] Y. Liu, S. Baumann, F. Schulze-Küppers, D.N. Mueller, O. Guillon, Co and Fe co-doping influence on functional properties of $SrTiO_3$ for use as oxygen transport membranes, Journal of the European Ceramic Society 38(15) (2018) 5058-5066.

[39] E. Forster, D. van Holt, M.E. Ivanova, S. Baumann, W.A. Meulenberg, M. Müller, Stability of ceramic materials for H_2 transport membranes in gasification environment under the influence of gas contaminants, Journal of the European Ceramic Society 36 (2016) 3457–3464.

[40] J. Drowart, C. Chatillon, J. Hastie, D. Bonnell, High-temperature mass spectrometry: Instrumental techniques, ionization cross-sections, pressure measurements, and thermodynamic data (IUPAC Technical Report), Pure and Applied Chemistry, 2005, p. 683.

[41] K. Hilpert, R. Ruthardt, Determination of the Dissociation Energy of the Cr_2 Molecule, Berichte der Bunsengesellschaft für physikalische Chemie 91(7) (1987) 724-731.

[42] M. Oku, Y. Sato, In-situ X-ray photoelectron spectroscopic study of the reversible phase transition between CoO and Co_3O_4 in oxygen of 10^{-3} Pa, Applied Surface Science 55(1) (1992) 37-41.

[43] M. Morales, F. Espiell, M. Segarra, Performance and stability of $La_{0.5}Sr_{0.5}CoO_{3-\delta}$ perovskite as catalyst precursor for syngas production by partial oxidation of methane, International Journal of Hydrogen Energy 39(12) (2014) 6454-6461.

[44] J.F. Monteiro, A.A.L. Ferreira, I. Antunes, D.P. Fagg, J.R. Frade, Thermodynamic restrictions on mechanosynthesis of strontium titanate, Journal of Solid State Chemistry 185 (2012) 143-149.

[45] R.T. Grimley, R.P. Burns, M.G. Inghram, Mass-Spectrometric Study of the Vaporization of Cobalt Oxide, The Journal of Chemical Physics 45(11) (1966) 4158-4162.

[46] C.-Y. Tsai, A.G. Dixon, W.R. Moser, Y.H. Ma, Dense perovskite membrane reactors for partial oxidation of methane to syngas, Aiche J. 43(11A) (1997) 2741-2750.

[47] N.F. Dalleska, P.B. Armentrout, Guided ion beam studies of reactions of alkaline earth ions with O_2, Int. J. Mass Spectrom. Ion Processes 134 (1994) 203-212.